Crystal Structure of an EMAP-II-Like Cytokine Released from a Human tRNA Synthetase

by **Xiang-Lei Yang**[a]), **Jianming Liu**[a]), **Robert J. Skene**[b]), **Duncan E. McRee**[b]), and **Paul Schimmel***[a])

[a]) The Skaggs Institute for Chemical Biology and the Departments of Molecular Biology and Chemistry, The Scripps Research Institute, BCC-379, 10550 North Torrey Pines Road, La Jolla, CA 92037, USA (phone: +1 858 784 8970; fax: +1 858 784 8990; e-mail: schimmel@scripps.edu)

[b]) Syrrx, Inc., 10410 Science Center Drive, San Diego, CA 92121, USA

Dedicated to Professor *Jack D. Dunitz* on the occasion of his 80th birthday

Aminoacyl-tRNA synthetases catalyze the first step of protein synthesis by aminoacylation of tRNAs. Remarkably, biological fragments of two human enzymes – tyrosyl-tRNA synthetase (TyrRS) and tryptophanyl-tRNA synthetase – are active cytokines produced by proteolysis or alternative splicing. One is a C-terminal fragment of TyrRS (C-TyrRS) that has potent activity for chemotaxis of leukocytes and monocytes and for stimulating production of other cytokines. Significantly, the cytokine activity of C-TyrRS is absent in the context of the full-length native protein. Unknown is the mechanism by which domain-release from the dimeric native protein activates the cytokine. Here, the crystal structure of C-TyrRS is presented at 2.2 Å resolution. This structure is similar to that of endothelial monocyte-activating protein II (EMAP-II), with critical residues of a heptapeptide element important for chemotaxis activity exposed on the first strand of a β-barrel of the monomeric unit. In contrast, the same residues of C-TyrRS are buried in an operational model for native TyrRS. Importantly, C-TyrRS is shown here to be monomeric when released from dimeric native TyrRS. Further analysis suggests that the critical residues are exposed when tRNA is bound. Thus, tRNA binding to native TyrRS may be an additional or alternative way to activate cytokine signaling.

Introduction. – Although aminoacyl-tRNA synthetases are well-known for their universal role in protein synthesis [1–3], other functions for these proteins are now established. These functions include regulation of transcription and translation [4][5], promotion of RNA splicing [6–9], and participation in pathways for RNA trafficking [10][11] and for signal transduction [12–19]. Two homologous synthetases – tyrosyl- and tryptophanyl-tRNA synthetase (TyrRS and TrpRS) – are active in cytokine signaling pathways, including those for angiogenesis and inflammation [12–19]. TyrRS is secreted under apoptotic conditions and can be cleaved by an extracellular protease, such as leukocyte elastase [12]. The resulting two fragments – the N-terminal mini-TyrRS that contains the catalytic body and the C-terminal domain (C-domain or C-TyrRS) that is homologous to the endothelial monocyte-activating protein II (EMAP-II) – have distinct cytokine activities. In particular, mini-TyrRS is an interleukin-8-like cytokine that binds to the CXC-type A receptor [12]. C-TyrRS has EMAP-II-like activity for chemotaxis of leukocytes and monocytes and for stimulating production of tissue factor, myeloperoxidase, and tumor necrosis factor α [12][13]. Strikingly, these activities are masked in full-length TyrRS.

The EMAP-II-like C-terminal domain is not found in TyrRS orthologs of lower eukaryotes, archaebacteria, or prokaryotes (*Fig. 1*) [20]. Similarly, the cytokine activity

of mini-TyrRS depends on a critical ELR tripeptide that is absent from the orthologs of prokaryotes and lower eukaryotes [13]. Thus, in the evolution of tRNA synthetases, such as TyrRS, the acquisition of the cytokine functions associated with critical motifs accompanied the appearance of higher eukaryotes.

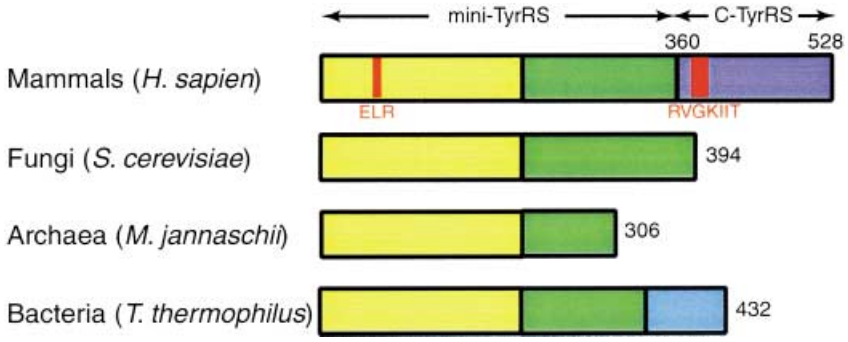

Fig. 1. *Illustration of the organization of domains of TyrRS enzymes.* All TyrRS have a catalytic *Rossmann*-fold domain (yellow) and an anticodon-recognition domain (green). In addition, human TyrRS has an EMAP-II-like C-terminal domain (purple) not found in TyrRS of fungi, archaea, or bacteria. In contrast, bacterial TyrRS has a smaller C-terminal domain (blue), which is distinct from that of human TyrRS. The critical ELR tripeptide and RVGKIIT heptapeptide for cytokine activities of mini-TyrRS and C-TyrRS, respectively, are highlighted in red on human TyrRS.

Recently, we reported the structure of mini-TyrRS at a resolution of 1.18 Å [21]. The critical ELR motif is part of the catalytic domain that, in turn, is joined to a domain that interacts with the tRNA anticodon. Both domains are part of mini-TyrRS. Significantly, the catalytic domain of the human protein can be superimposed on those of its bacterial counterparts. In contrast, the anticodon-recognition domain of the human enzyme has a unique orientation relative to the position of the catalytic domain in the structures of the bacterial orthologs. This unique disposition of the anticodon-recognition domain in the human enzyme can explain why mini- and not full-length TyrRS is an active cytokine. In particular, the C-terminal domain of human TyrRS is fused to the anticodon-recognition domain in a position that sterically blocks the ELR motif. Were the anticodon-recognition domain positioned like that in the bacterial orthologs, the ELR motif would not be blocked.

Here, we set out to visualize the structure and understand the activation of C-TyrRS that occurs on splitting of the full-length protein. In addition to EMAP-II, whose structure has been reported [22][23], the C-domain is homologous to the structure-specific tRNA-binding protein Trbp111 [24–27] and to Trbp111-like CsaA [28], to Arc1p (which plays a role in nuclear trafficking of tRNA in yeast) [29], and to the C-terminal domain of specific methionyl-tRNA synthetases [30][31]. Although they are homologous proteins, EMAP-II is a monomer in solution, while Trbp111 and CsaA are dimers. Also, the cloned C-terminal domain of the *Pyrococcus abyssi* MetRS homolog is dimeric [31]. Thus, in addition to determining the structure of C-TyrRS, the question of whether the C-domain is monomeric (like EMAP-II) or dimeric (like both Trbp111 and CsaA) was of interest. In particular, we imagined that dimerization *per se* could be important for quenching the cytokine activity of C-TyrRS. In this regard, it is

noteworthy that both mini- and full-length TyrRS are dimeric. Thus, we set out to investigate the oligomeric state of C-TyrRS once released from the dimeric native enzyme and to obtain C-TyrRS crystals for high-resolution structure analysis.

Results and Discussion. – *C-TyrRS as a Monomer.* Although some pseudo dimers were observed in the crystal lattice (see below), gel-filtration experiments with samples of full-length TyrRS, mini-TyrRS, and C-TyrRS showed that C-TyrRS is a monomer of *ca.* 20-kD molecular weight. In contrast, mini- and full-length TyrRS are dimers (*Fig. 2,a*). Dimerization of the latter two proteins occurs because of a specific dimer interface imbedded in the N-terminal *Rossmann*-fold domain. This interface was clearly resolved in the crystal structure of mini-TyrRS [21]. While the homologs Trbp111, the Trbp111-like protein CsaA, and the C-terminal domain of some bacterial MetRS enzymes are tight dimers [25][28][31], EMAP-II and the EMAP-II-like C-terminal domain of plant MetRS appear to be monomers in solution [22][23][30]. Thus, when C-TyrRS is released from native TyrRS, it adopts the monomeric form seen with EMAP-II and not the dimeric state found in certain of the homologs that are not known to be cytokines.

Crystal Packing. Recombinant C-TyrRS crystallized in the *P*1 space group. There were four copies of C-TyrRS (**A**, **B**, **C**, **D**) in a unit cell of dimensions $54.6 \times 59.5 \times 71.6$ Å (*Fig. 2,b*). Molecule **A** was close to the same orientation as molecule **B**, while **C** was close to the orientation of **D**. In addition, **C** is related to each **A** and **B** by a pseudo-2-fold symmetry, while **D** is related to each **A** and **B** by a pseudo-2-fold screw symmetry. Extensive intermolecular interactions prevented C-TyrRS from crystallizing in a higher-symmetry space group. For example, the N-termini of **A**, **B**, **C**, and **D** bind in the cleft between a β-strand (β9) and the loop before the 3_{10} helix designated as η2 (*Fig. 3,a*, see below) of **C**, **D**, **A**, and **B**, respectively, either from the same or adjacent unit cells.

Description of the C-TyrRS Structure. All four molecules in the unit cell have similar conformations. The rms deviations between the C_α-atoms of the four molecules were in the range of 0.15 – 0.29 Å, with **A** being closer in conformation to **B**, and **C** closer to **D** (*Fig. 2,b*). Differences are mainly confined to loop regions, *e.g.*, the most-obvious difference between **A**/**B** and **C**/**D** is at the turn between β9 and β10, encompassing Pro^{100} to Gly^{102} (*Fig. 3,a*, see below).

The structure of C-TyrRS (171 amino acid residues) can be divided into two closely interacting domains. The first is a β-barrel (extending from Pro^{2} to Leu^{82}) that resembles an oligonucleotide-binding (OB) fold (*Fig. 3,a*). This domain consists of seven β-strands ($\beta1-\beta7$) and two short 3_{10} helices, with the first (η1) at the N-terminus and η2 fitting between β3 and β4. Two antiparallel β-sheets ($\beta1-\beta2-\beta3$ and $\beta1-\beta4-\beta7$) form the core of the β-barrel, the $\beta5-\beta6$ hairpin being in a flanking position, and the helix η2 capping the β-barrel.

The second domain extends from Leu^{83} to Glu^{172} (*Fig. 3,a*). The core of the second domain consists of two antiparallel β-sheets ($\beta10-\beta13-\beta14$ and curved $\beta9-\beta8-\beta15-\beta11-\beta12$) with a long loop between β9 and β10, joining the two sheets together (*Fig. 3,a*). Another long loop and two helices (η3 and α1 between β10 and β11) make a 270 degree cycle and wrap around the η1 helix of the first domain. Overall, the second

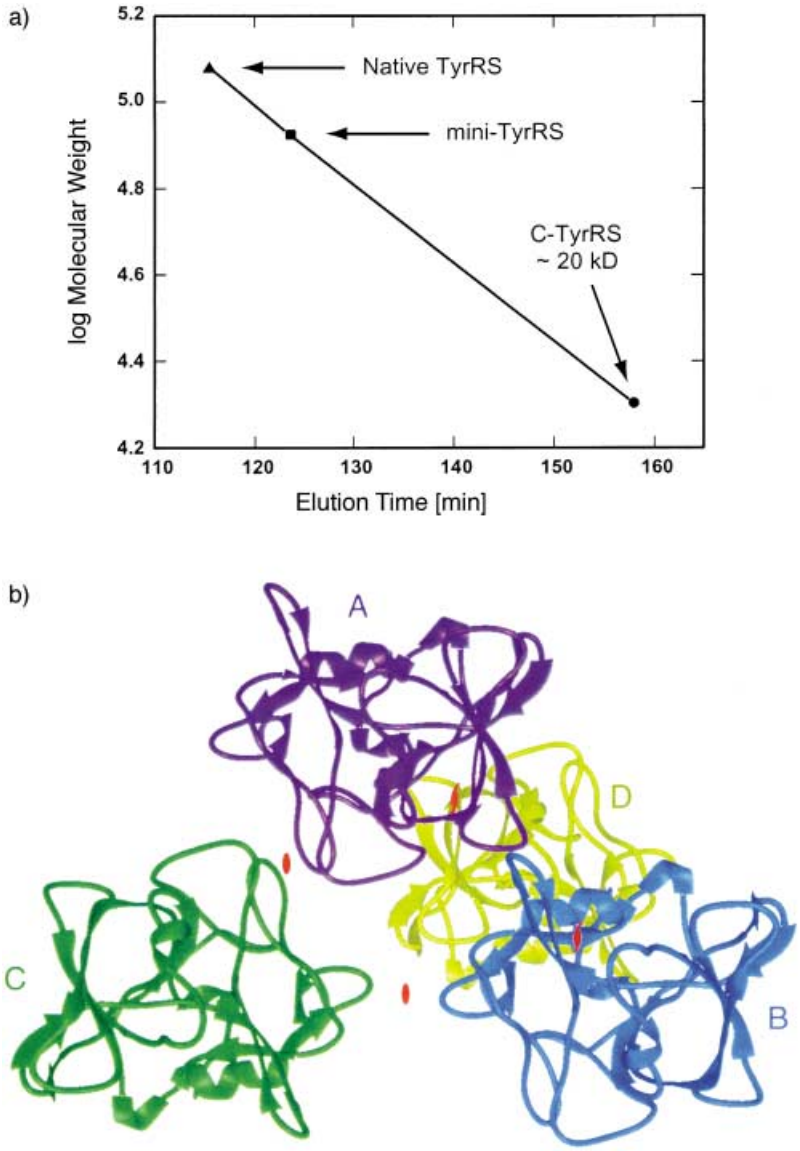

Fig. 2. *a*) Superose-12 *gel filtration of samples of full-length TyrRS, mini-TyrRS and C-TyrRS*. The estimated molecular weights are consistent with full-length TyrRS and mini-TyrRS dimers, as well as monomeric C-TyrRS. *b*) *Crystal packing of four C-TyrRS molecules* (**A**, **B**, **C**, **D**) *in the unit cell*. Molecule **A** (purple) is orientated similar to molecule **B** (blue), while **C** (green) has a similar orientation to that of **D** (yellow). In addition, **C** is related to each **A** and **B** by pseudo-2-fold symmetry, while **D** is related to each **A** and **B** in the unit-cell by pseudo-2-fold screw symmetry. In this paper, all figures of molecular structures were generated with MIDAS (University of California, San Francisco).

domain joins together like a bowl to support the OB fold β-barrel of the first domain (*Fig. 3*,*a*). The two domains are tightly linked together between β7 and β8.

The sequence of human C-TyrRS (171 residues) aligns with that of human EMAP-II with an identity of 50% and a similarity of 68%. As anticipated, the structure of C-TyrRS is similar to that of EMAP-II (PDB code 1FL0) with an rms deviation of only 1.11 Å for 163 of the C_α-atoms (*Fig. 3*,*b* and *3*,*c*). Besides some loop regions, the main differences between C-TyrRS and EMAP-II are at strands β8, β10, and strand β15 at the C-terminus. The C-terminus seems to be flexible even as part of a curved β-sheet ($\beta9-\beta8-\beta15-\beta11-\beta12$).

In analyzing the structure of C-TyrRS, we define the first domain as extending to the end of β7, which demarks the limit of the β-barrel. (In the recently reported structure of EMAP-II [23], the first domain was defined as extending to β9, thus, going beyond the β-barrel of the OB fold. In addition, β8 and β9 are part of the core β-sheet ($\beta9-\beta8-\beta15-\beta11-\beta12$) of the second domain and, therefore, seem more appropriately assigned to that domain). As seen with the structure of EMAP-II [22][23], the OB fold closely resembles the OB fold of each monomer that makes up the Trbp111 dimer, whereas the second domain mimics the dimerization region in the Trbp111 dimer. Specifically, the face of the monomer that forms the dimer interface in Trbp111 is buried in a C-terminal piece (Val^{111} to Glu^{172}) of the second domain of C-TyrRS. This C-terminal piece is absent from Trbp111 (*Fig. 3*,*c*) and blocks the formation of the dimer interface. Therefore, unlike Trbp111, C-TyrRS and EMAP-II cannot form dimers.

Location of the Heptapeptide with Chemotaxis Activity. The heptapeptide RVGKIIT (Arg^{13}–Thr^{19}) was shown previously to have chemotaxis activity for mononuclear phagocytes and polymorphonuclear leukocytes [13]. This peptide is located on the β1-strand of the β-barrel of the first domain. Similar to what was observed with the EMAP-II structure, the Arg^{13}, Val^{14}, and Ile^{17} side chains are more or less buried, but the side chains of Lys^{16}, Ile^{18} and Thr^{19} are well-exposed. The exposure of Ile^{18} and Thr^{19} is consistent with the results of chemotaxis assays on heptapeptides derived from different EMAP-II homologs. These experiments showed that the last two residues of the heptapeptide are critical for activity [13]. Therefore, Ile^{18} and Thr^{19} in C-TyrRS are likely to play an important role in receptor binding.

Potential Mechanism for Cytokine Activation by Cleavage of Native TyrRS. This work, together with the recently reported structure of mini-TyrRS [21], provides some of the essential details needed to understand how two cytokines are activated upon being released from native TyrRS. For example, the critical tripeptide ELR for the cytokine activity is essentially exposed in the mini-TyrRS structure. Similarly, the

Fig. 3. a) *Stereoview of the C-TyrRS structure.* The first β-barrel domain is in purple, and the second domain is in cyan. The critical heptapeptide RVGKIIT (red) for cytokine activity of C-TyrRS is located on the β1 strand of the first domain. The positions of Ser^{78} and Met^{81} potentially involved in tRNA binding are marked by golden triangles. b) *Superpostion of C-TyrRS structure* (colored) *with EMAP II structure* (gray). The coloring scheme for C-TyrRS is the same as in *a*). c) *Structural alignment of C-TyrRS with human EMAP II,* Aquifex aeolicus *Trbp111 and* Thermus thermophilus *CsaA*. The domain separation and the secondary structure of C-TyrRS are superimposed on top (β/β-strand, α/α-helix, $\eta/3_{10}$ helix, TT/β-turn). The extra C-terminal piece in C-TyrRS and EMAP II that blocks formation of the dimer interface is annotated. Ser^{78} and Met^{81} on C-TyrRS (equivalent to Ser^{82} and Met^{85} on Trbp111 involved in tRNA binding) are highlighted by golden triangles. The alignment was generated by DALI [42] and drawn with ESPript [43]. Identical residues are highlighted in red, and similarities are shown in pink. →

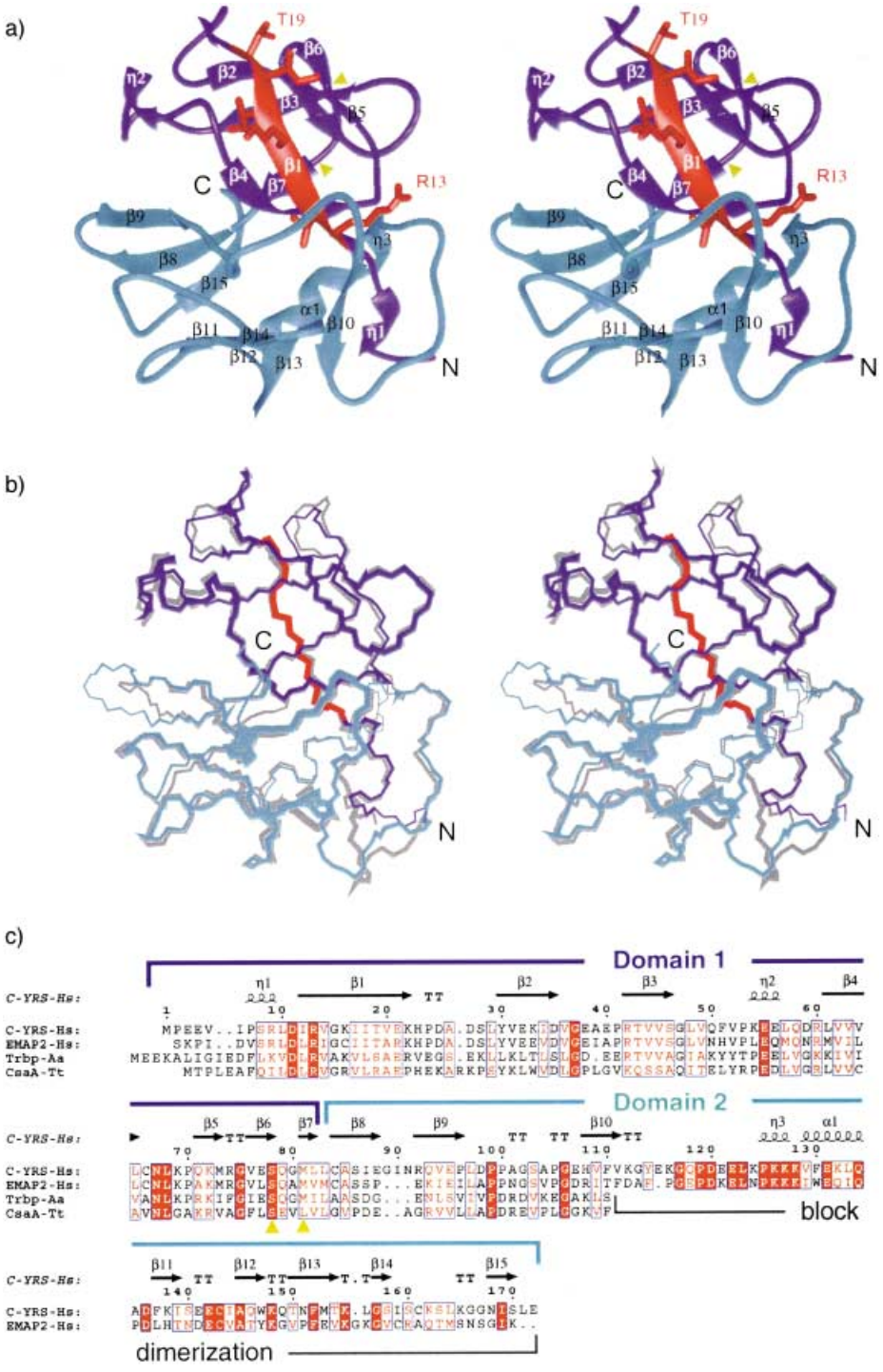
a)
T19
β6
β2
η2
β3
β5
β1
C
β4
β7
R13
β9
η3
β8
β15
α1
β11
β14
β10
η1
β12
β13
N
b)
C
N
c)
Domain 1
Domain 2
C-YRS-Hs:
C-YRS-Hs: MPEEV..IPSRLDIRVGKIITVEKHPDA.DSLYVEKIDVGEAEPRTVVSGLVQFVPKDELQDRLVVV
EMAP2-Hs: SKPI..DVSRLDLRIGCIITAREKHPDA.DSLYVEEVDVGEIAPRTVVSGLVNHVPLEQMQNRMVIL
Trbp-Aa MEEKALIGIEDFLKVDLRVAKVLEAERVEGS.EKLLKLTLSLGD.EEPTVVAGIAKYYTPEELVGKKIVI
CsaA-Tt MTPLEAFQIIDLRVGRVLRAEPHEKARKPSYKLWVDLGPLGVKQSSAQITELYRPEDLVGRLVVC
block
dimerization

critical residues in the aforementioned heptapeptide are exposed in the structure of C-TyrRS. Because the cytokine activities of both mini-TyrRS and C-TyrRS are absent in full-length TyrRS, we speculate that those critical residues are masked when mini-TyrRS and C-TyrRS are joined together in the native enzyme (whose structure is not known). Indeed, the trajectory of the C-terminal end of mini-TyrRS is such that the C-domain would be placed in a position to block or cover the ELR motif.

For the purpose of having an operational model for native TyrRS, we started by focusing on an unresolved linker of 17 residues (in the crystal of mini-TyrRS) that lies between the C-terminus of mini-TyrRS and the N-terminus of the C-TyrRS segment within native TyrRS. Two secondary-structure-prediction programs, PSA [32][33] and PHD [34][35], suggested that this region forms loops or turns that are flexible. Leukocyte elastase cleaves the native TyrRS at this loop region and releases mini-TyrRS and C-TyrRS. This flexible linker can also control the spatial orientation of C-TyrRS relative to mini-TyrRS (within the native enzyme). In one orientation sterically allowed, a negatively charged patch associated with the critical heptapeptide of C-TyrRS is brought 'face-to-face' with the positive surface that surrounds the ELR motif of mini-TyrRS (see below). With this orientation of the two domains of native TyrRS, the determinants for cytokine activities are sequestered.

Potential Mechanism for Cytokine Activation without Cleavage of Native TyrRS. The above analysis assumes that activation occurs in the absence of bound tRNA. Indeed, experimental studies of activation of C-TyrRS have been performed in the absence of added tRNA, suggesting that a tRNA cofactor is not needed [12]. However, we considered an additional or alternative mechanism for activation of native TyrRS that might occur without splitting TyrRS. This alternative was based on the idea that $tRNA^{Tyr}$ could be a cofactor needed for unmasking the critical determinants in the native enzyme.

For this purpose, we took advantage of the structure of the complex of TyrRS with $tRNA^{Tyr}$ from *Thermus thermophilus* [36]. Because of the structural homology of the *Rossmann*-fold domain of human and *T. thermophilus* TyrRS, we were able to construct a model for the mini-TyrRS/tRNA complex by superimposing the central β-strands of the two *Rossmann* folds (human and *T. thermophilus* proteins, rms deviation of 1.94 Å for 50 C_α-atoms). For each tRNA bound to the dimer, the acceptor stem interacts with the *Rossmann*-fold domain of one monomer, while the anticodon stem/loop interacts with the anticodon-recognition domain of the other monomer. Mini-TyrRS had no steric clashes with $tRNA^{Tyr}$ in the model generated.

As for the interaction of tRNA with the C-TyrRS domain, we took advantage of the crystal structure of Trbp111 docked onto the outer, convex side of the L-shaped tRNA corner [25]. (Trbp111 is a dimeric, structure-specific tRNA-binding protein that interacts specifically with the outside corner of tRNA). Ser^{82} and Met^{85} of Trbp111 are important for interactions of Trbp111 with tRNA [25]. Both residues are conserved in C-TyrRS. They are located at the end of β6 and beginning of β7, respectively (*Fig. 3,a* and *3,c*). We superimposed C-TyrRS onto the Trbp111 monomer, which has side chains of Ser^{82} and Met^{85} in contact with tRNA (rms deviation of 1.68 Å for 99 C_α-atoms). To test this model, we confirmed that the electrostatic distribution at the surface of C-TyrRS is consistent with a tRNA interaction (*Fig. 4,c*). Specifically, an area with strong positive potential (blue) on C-TyrRS is close to the negatively charged tRNA

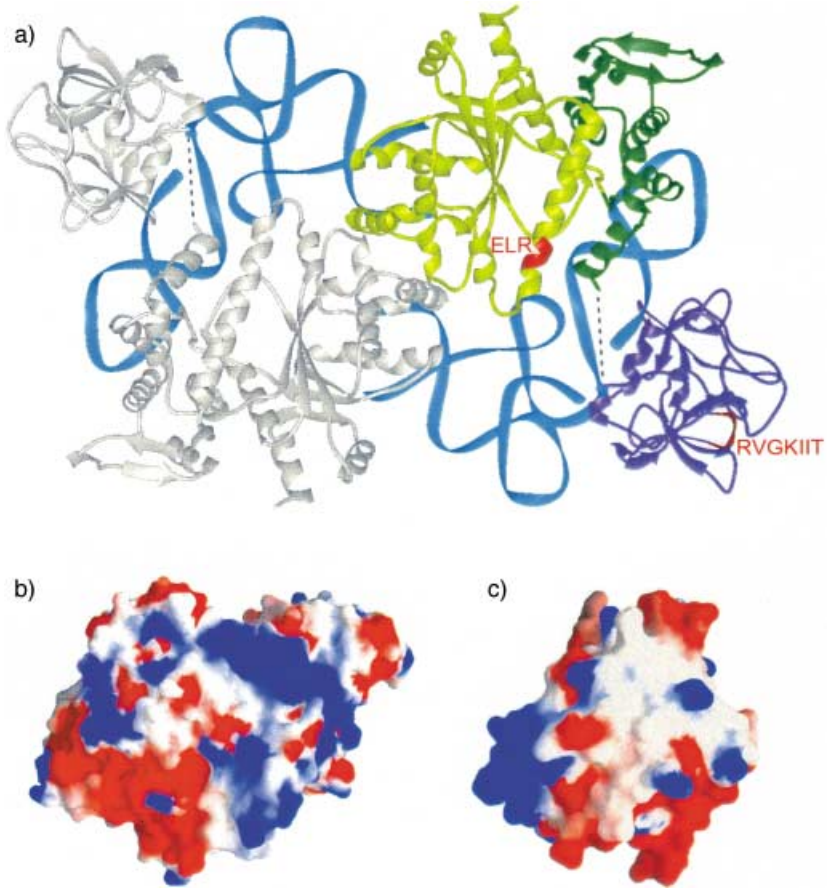

Fig. 4. a) *A model of human TyrRS as a complex with tRNA. Rossmann* fold, anticodon recognition, and C-terminal domains of one TyrRS monomer are colored in yellow, green, and purple, respectively. tRNA Molecules are colored in cyan. The ELR tripeptide and the RVGKIIT heptapeptide are highlighted in red. b), c) *Surface electrostatic potential of mini-TyrRS and C-TyrRS, respectively, with positive potential in blue and negative potential in red*. Images were generated by GRASP [44]. The orientations in *b*) and *c*) are as in *a*) for the colored monomers of mini-TyrRS and C-TyrRS, respectively.

backbone. This positively charged area is located around helix $\eta 3$ from the second domain of C-TyrRS (*Fig. 3*,*a*).

Finally, tRNA from the model of the complex with mini-TyrRS was superimposed with tRNA from the model of its complex with C-TyrRS. This superposition brought together the two fragments of TyrRS (*Fig. 4*,*a*). In this model, mini-TyrRS binds to the inner, concave side of tRNA (as is the case in typical synthetase-tRNA complexes [37][38]), whereas C-TyrRS binds to the outer corner on the opposite side (as in the case with Trbp111 binding to tRNA [25]). The N-terminus of C-TyrRS is separated from the C-terminus of mini-TyrRS by 17 Å, a distance that is reasonable for the 17 unresolved residues between mini-TyrRS and C-TyrRS. The cytokine-active RVGKIIT heptapeptide on C-TyrRS is located on the opposite side of the tRNA-binding face (*i.e.*,

$\eta 3$, $\beta 6-\beta 7$; *Fig. 3,a*), and has negative (red) electrostatic potential (*Fig. 4,c*). The heptapeptide on C-TyrRS and the ELR tripeptide in mini-TyrRS are each exposed in the human TyrRS/tRNA complex. Thus, both critical peptide determinants are potentially available for receptor interactions when tRNA is bound to the native enzyme.

Because full-length TyrRS is no active cytokine, we speculate that a major conformational change in the 17-residue linker region occurs upon tRNA binding. This change would prevent two positively charged tRNA binding surfaces from collapsing onto each other. For example, C-TyrRS might rotate about 180 degrees and use the negatively charged side of the heptapeptide to interact with the ELR region of mini-TyrRS. Indeed, the ELR region on mini-TyrRS has positive (blue) electrostatic potential that is 'complementary' to the negative (red) potential around the heptapeptide (*Fig. 4,b*). Thus, both determinants for cytokine activities would be masked in full-length TyrRS, as we speculated earlier (*vide supra*) [21].

Conclusions. – The models for cytokine activation presented above give rise to the same end result by two distinct mechanisms (*Fig. 5*). In native TyrRS, the ELR motif of mini-TyrRS and the critical heptapeptide of C-TyrRS are effectively 'face-to-face' and unable to interact with their respective receptors. Direct cleavage of the linker region between mini-TyrRS and C-TyrRS provides a simple mechanism for exposing the critical determinants needed for cytokine activity. In the presence of tRNA, a conformational change could, in principle, activate the cytokines imbedded in native TyrRS. (All studies of cytokine activation reported so far have not employed tRNA as an added cofactor). Thus, from this perspective, tRNA binding might be an additional or alternative mechanism for activating the imbedded cytokines of human TyrRS. We are currently investigating this hypothesis by directly testing whether addition of

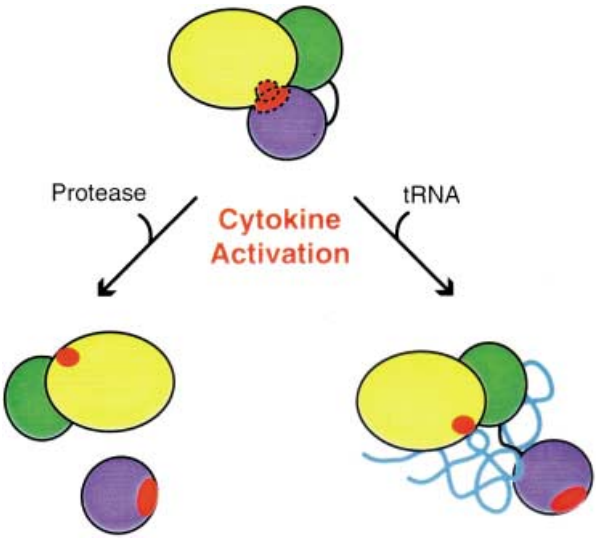

Fig. 5. *Illustration of two possible mechanisms for cytokine activation of human TyrRS*

$tRNA^{Tyr}$ can activate native TyrRS in cell-based assays. At the same time, efforts are also being directed at obtaining a structure of native TyrRS in the presence and absence of $tRNA^{Tyr}$.

Experimental Part

Protein Expression, Purification, and Characterization. The plasmid containing the gene for C-TyrRS was described previously [12]. C-TyrRS was expressed in *E. coli* and purified to homogeneity (> 95% pure by SDS PAGE) by Ni-NTA, ion-exchange (*Mono-Q*) chromatography (*Pharmacia Biotech*, Piscataway, NJ), as stated before [18]. Gel-filtration experiments were performed using a *Superose-12* column (*Pharmacia Biotech*).

Crystallization by Means of High-Throughput Screening. C-TyrRS (6 mg/ml) was maintained in a stock soln. of 10 mM *Hepes* (pH 7.5), 20 mM KCl, 0.02% NaN_3, and 2 mM β-mercaptoethanol. Initial crystallization

Table. *Crystal Data and Structure-Refinement Statistics*

Crystal Data:	
Wavelength [Å]	1.542
Molecular weight [g mol^{-1}]	19923
Crystal system	Triclinic
Space group	*P*1
Z	4
a [Å]	54.6
b [Å]	59.5
c [Å]	71.6
α [°]	103.5
β [°]	110.0
γ [°]	101.5
V [$Å^3$]	196801
Solvent content [%]	50.2
Resolution [Å]	2.2
Unique reflections	39281
Completeness [%][a])	94.6 (83.7)
Redundancy	3.7
R_{merge} [%][a]) [b])	6.7 (25.2)
$\langle I/\sigma(I)\rangle$ [a])	18.7 (3.8)
Refinement Statistics:	
Resolution range [Å]	20–2.2
Number of reflections (working / free)	33987 / 1786
Number of atoms (protein / water)	5320 / 182
R_{work} / R_{free} [%][c])	25.1 /29.6
rms deviation bond length [Å]	0.006
rms deviation bond angle [°]	1.54
Ramachandran plot [%]	
favored	86.9
allowed	13.1
generously allowed	0.0
disallowed	0.0
Average *B*-factors for protein [$Å^2$]	36.5
Average *B*-factors for waters [$Å^2$]	34.7

[a]) Numbers in parentheses refer to the highest resolution shell. [b]) $R_{merge} = (\Sigma_h\Sigma_i | I_i(h) - \langle I(h)\rangle | / \Sigma_h\Sigma_i I_i(h)) \times 100$, where $\langle I(h)\rangle$ is the average intensity of *I* symmetry-related observations of reflections with a *Bragg* index *h*. [c]) $R_{work} = (\Sigma_{hkl} | F_o - F_c | / \Sigma_{hkl} | F_o |) \times 100$, where F_o and F_c are the observed and calculated structure factors, respectively, for 95% of the randomly selected reflections used in the refinement. R_{free} was calculated as for R_{work}, but on 5% of the reflections excluded before refinement. Numbers refer to all data.

trials of C-TyrRS were conducted using the proprietary high-throughput protein crystallization platform developed at *Syrrx*, *Inc.* (La Jolla, CA). The crystallization experiments were set up on the *Agincourt* crystallization robot using patented submicroliter crystallization technology. For both protein samples, a sparse matrix approach was employed under a suite of 480 unique crystallization conditions at temps. of 20° and 4°. In addition, 480 systematic conditions using different precipitants, such as $(NH_4)_2SO_4$ (0.5–2.8 M), polyethyleneglycol-500 monomethyl ether (PEG MME 500; 10–40%), PEG MME 2000 (6–24%), PEG MME 5000 (5–20%), PEG 8000 (5–20%), and 2-methylpentane-2,4-diol (6–40%) at pH 4–9 were set up. Each crystallization plate contained 96 sitting-drop experiments on which each drop of a 50-nl protein sample was mixed with an equal volume of reservoir soln. The setups were subsequently incubated and automatically imaged at regular intervals. Using this technology, a total of 1,920 crystallization samples were set up over a two-hour period, with a total of 200 µl of C-TyrRS protein sample. Productive crystallization conditions were then repeated using 2 µl protein sample plus 2 µl reservoir sitting-drops. C-TyrRS usually grew into crystal bundles in a few days from the reservoir containing 2.8M $(NH_4)_2SO_4$, 0.1M NaH_2PO_4/K_2HPO_4 (pH 6.9), and 2% acetone at 4°. Microseeding was needed to obtain plank-like single crystals with a maximal size of $0.1 \times 0.2 \times 0.8$ mm.

Data Collection, Structure Determination and Refinement. X-Ray data from a flash-frozen crystal were collected on a *MAR345* imaging plate (*MAR USA*, Evanston, IL) using rotating anode X-rays. Data were integrated and scaled with HKL2000 [39]. The structure was solved by molecular replacement using the structure of EMAP-II (PDB code 1FL0) as the initial search model. Two top solns. were found in the self-rotation search, with each giving two top solutions in the following translation search. Altogether, four molecules were found in the *P*1 unit cell. Rotation and translation searches were conducted in CNS [40], on data in the range of 20 – 4 Å. The structure was refined by cycles of manual model adjustment using O [41], and simulated-annealing refinement was performed with the aid of CNS. Noncrystallographic symmetry was applied throughout the refinement, except for the final phase. Data collection and refinement statistics are summarized in the *Table*. The atomic coordinates and structure factors have been deposited in the *Protein Data Bank*, www.rcsb.org (PDB ID code lNTG).

We thank *Dr. Xiaoping Dai* for help with X-ray data collection and *Dr. Marc Elsliger* for assistance with computer software. This work was supported by grants GM15539 and CA92577 from the *National Institutes of Health* and *The National Cancer Institute*, respectively, as well as by a fellowship from *The National Foundation for Cancer Research*.

REFERENCES

[1] R. Giége, J. D. Puglisi, C. Florentz, *Prog. Nucl. Acid Res. Mol. Biol.* **1993**, *45*, 129.
[2] C. W. Carter Jr., *Ann. Rev. Biochem.* **1993**, *62*, 715.
[3] M. Ibba, D. Söll, *Ann. Rev. Biochem.* **2000**, *69*, 617.
[4] S. D. Putney, P. Schimmel, *Nature (London)* **1981**, *291*, 632.
[5] H. Putzer, M. Grunberg-Manago, M. Springer, in 'tRNA: Structure, Biosynthesis and Function', Eds. D. Söll, U. RajBhandary, ASM Press, Washington, DC, 1995, p. 293–333.
[6] A. M. Lambowitz, P. S. Perlman, *Trends Biochem. Sci.* **1990**, *15*, 440.
[7] G. Dujardin, C. J. Herbert, in 'Ribosomal RNA and Group I Introns', Eds. R. Green, R. Schroeder, Lands Bioscience, Austin, TX, 1997, p. 179–198.
[8] S. B. Rho, S. A. Martinis, *RNA* **2000**, *6*, 1882.
[9] C. A. Myers, B. Kuhla, S. Cusack, A. M. Lambowitz, *Proc. Natl. Acad. Sci. U.S.A* **2002**, *99*, 2630.
[10] E. Lund, J. Dahlberg, *Science* **1998**, *282*, 2082.
[11] S. Sarkar, A. K. Hopper, *Mol. Biol. Cell* **1998**, *9*, 3041.
[12] K. Wakasugi, P. Schimmel, *Science* **1999**, *284*, 147.
[13] K. Wakasugi, P. Schimmel, *J. Biol. Chem.* **1999**, *274*, 23155.
[14] K. Wakasugi, B. Slike, M. J. Hood, K. L. Ewalt, D. A. Cheresh, P. Schimmel, *J. Biol. Chem.* **2002**, *277*, 20124.
[15] K. Wakasugi, B. M. Slike, J. Hood, A. Otani, K. L. Ewalt, M. Friedlander, D. A. Cheresh, P. Schimmel, *Proc. Natl. Acad. Sci. U.S.A.* **2002**, *99*, 173.
[16] A. Otani, B. M. Slike, M. I. Dorrell, J. Hood, K. Kinder, K. L. Ewalt, D. Cheresh, P. Schimmel, M. Friedlander, *Proc. Natl. Acad. Sci. U.S.A.* **2002**, *99*, 178.
[17] K. L. Ewalt, P. Schimmel, *Biochemistry* **2002**, *41*, 13344.
[18] J. Liu, X.-L. Yang, K. L. Ewalt, P. Schimmel, *Biochemistry* **2002**, *41*, 14232.
[19] A. Otani, K. Kinder, K. Ewalt, F. J. Otero, P. Schimmel, M. Friedlander, *Nat. Med.* **2002**, *8*, 1004.

[20] T. A. Kleeman, D. Wei, K. L. Simpson, E. A. First, *J. Biol. Chem.* **1997**, *272*, 14420.
[21] X.-L. Yang, R. J. Skene, D. E. McRee, P. Schimmel, *Proc. Natl. Acad. Sci. U.S.A* **2002**, *99*, 15369.
[22] Y. Kim, J. Shin, R. Li, C. Cheong, K. Kim, S. Kim, *J. Biol. Chem.* **2000**, *275*, 27062.
[23] L. Renault, P. Kerjan, S. Pasqualato, J. Menetrey, J. C. Robinson, S. Kawaguchi, D. G. Vassylyev, S. Yokoyama, M. Mirande, J. Cherfils, *EMBO J.* **2001**, *20*, 570.
[24] A. J. Morales, M. A. Swairjo, P. Schimmel, *EMBO J.* **1999**, *18*, 3475.
[25] M. A. Swairjo, A. J. Morales, C. C. Wang, A. R. Ortiz, P. Schimmel, *EMBO J.* **2000**, *19*, 6287.
[26] T. Nomanbhoy, A. J. Morales, A. T. Abraham, C. S. Vortler, R. Giége, P. Schimmel, *Nat. Struct. Biol.* **2001**, *8*, 344.
[27] T. Kushiro, P. Schimmel, *Proc. Natl. Acad. Sci. U.S.A.* **2002**, *99*, 16631.
[28] S. Kawaguchi, J. Muller, D. Linde, S. Kuramitsu, T. Shibata, Y. Inoue, D. G. Vassylyev, S. Yokoyama, *EMBO J.* **2001**, *20*, 562.
[29] G. Simos, A. Segref, F. Fasiolo, K. Hellmuth, A. Shevchenko, M. Mann, E. C. Hurt, *EMBO J.* **1996**, *15*, 5437.
[30] M. Kaminska, M. Deniziak, P. Kerjan, J. Barciszewski, M. Mirande, *EMBO J.* **2000**, *19*, 6908.
[31] T. Crepin, E. Schmitt, S. Blanquet, Y. Mechulam, *Biochemistry* **2002**, *41*, 13003.
[32] C. M. Stultz, J. V. White, T. F. Smith, *Protein Sci.* **1993**, *2*, 305.
[33] J. V. White, C. M. Stultz, T. F. Smith, *Math. Biosci.* **1994**, *119*, 35.
[34] B. Rost, C. Sander, R. Schneider, *Comput. Appl. Biosci.* **1994**, *10*, 53.
[35] B. Rost, C. Sander, *Methods Mol. Biol.* **2000**, *143*, 71.
[36] A. Yaremchuk, I. Kriklivyi, M. Tukalo, S. Cusack, *EMBO J.* **2002**, *21*, 3829.
[37] A. Rich, P. R. Schimmel, *Nucl. Acid Res.* **1977**, *4*, 1649.
[38] J. Cavarelli, D. Moras, *FASEB J.* **1993**, *1*, 79.
[39] Z. Otwinowski, W. Minor, in 'Methods in Enzymology', Eds. C. W. Carter Jr., R. W. Sweet, Academic Press, San Diego, 1997, Vol. 276, p. 307 – 326.
[40] P. D. Adams, L. M. Rice, A. T. Brunger, *Curr. Opin. Struct. Biol.* **1998**, *8*, 606.
[41] T. A. Jones, J. Y. Zou, S. W. Cowan, M. Kjeldgaard, *Acta Crystallogr., Sect. A* **1991**, *47*, 110.
[42] L. Holm, C. Sander, *J. Mol. Biol.* **1993**, *233*, 123.
[43] P. Gouet, E. Courcelle, D. I. Stuart, F. Metoz, *Bioinformatics* **1999**, *15*, 305.
[44] B. Honig, A. Nicholls, *Science* **1995**, *268*, 1144.

Received February 6, 2003